Industry Science and Engineering Vol. 3 No. 9, 2026

Path-Following Control of an Underactuated AUV Using GPS-Based Geometric Error and Threshold-Limited PID

Kai Chen, Shengguo Liang, Xiaoyu Zhao*
Tianjin Hanhai Lanfan Marine Technology Co., Ltd., Tianjin 300457, China
**Corresponding Author*

Abstract: An underactuated autonomous underwater vehicle (AUV) cannot move laterally under direct control. Its large mass and inertia can lead to overshoot during heading corrections, while GPS positioning noise can cause high-frequency chattering. We propose a PID controller that uses GPS-based geometric error with error thresholding and output limiting, referred to here as threshold-limited PID. Horizontal-plane kinematic and dynamic models were established from the parameters of a 7 m-class vehicle. GPS latitude and longitude were converted to local east-north coordinates. Heron's formula then gave the perpendicular distance to the desired straight-line path, and a vector cross product identified the side of the path occupied by the AUV. The resulting signed error can be calculated without a vehicle model. To reduce unnecessary corrections and chattering caused by small GPS positioning errors, we introduced a 2 m error threshold and reset the stored controller states. Vehicle inertia was addressed by limiting the positional PID heading correction to 30° and adding anti-windup constraints. These constraints work with derivative action, which anticipates error changes and suppresses inertial oscillations, to reduce overshoot and repeated oscillations caused by inertial lag. Comparative MATLAB simulations and lake trials were used to evaluate the controller. In simulation, it eliminated path overshoot relative to conventional PID, improved convergence speed by approximately 43%, and substantially improved steady-state accuracy. For the lake trials, an in-house-developed AUV with X-configured rudders, a length of 7 m, and a mass of 1260 kg followed a four-waypoint piecewise-linear path. Large initial errors decreased rapidly, and the controller accommodated turns between path segments. Errors stayed within the threshold for 86.40% of the operating time. Within this band, the steady-state root mean square error was 0.96 m, indicating submeter steady-state path-following accuracy. Both tests showed rapid convergence and smooth motion with high steady-state accuracy. The controller handles the nonlinear motion and actuation constraints of heavy underactuated AUVs without an accurate dynamic model. This, together with its suitability for real-time embedded implementation, makes it useful for practical path-following tasks.

Keywords: Underactuated AUV; Path Following; GPS-Based Geometric Error; Threshold Filtering; Output-Limited PID

1. Introduction

Environmental monitoring, underwater resource exploration, waterway inspection, and underwater operations all make use of autonomous underwater vehicles (AUVs). Their ability to travel long distances without a crew and with low energy consumption has made them widely used in marine engineering [1,2]. For an underactuated AUV, surge propulsion and yaw actuation are the only means of controlling motion in the horizontal plane. There is no separate lateral actuator to move the vehicle back onto its path. Instead, the AUV must change heading and approach the path as it moves forward. The lag in this indirect response, combined with nonlinearity and underactuation, makes accurate, stable path following difficult: corrections can overshoot the path and develop into inertial oscillations. Many conventional controllers have been tested only in simulation. Their limited treatment of actual vehicle inertia and disturbances encountered in real water environments continues to hinder practical application [1,2].

The simplicity, reliability, and straightforward tuning of PID control explain its widespread use in underwater-vehicle path following. Its application to an underactuated AUV

nevertheless requires care. Without error screening, even small GPS positioning errors trigger repeated heading corrections, producing high-frequency chattering. At the other end of the error range, the integral term may continue to accumulate until windup occurs [3]. Vehicle inertia compounds this effect, causing the AUV to overshoot and oscillate repeatedly about the path [4]. If the output is left unconstrained, excessively large heading corrections can intensify the oscillation. Conventional PID also lacks a means of using path geometry to determine which way to correct the heading, which limits its response to changing conditions.

Previous attempts to overcome these problems include fuzzy PID, adaptive PID, and integral-separation PID [5,6]. Most have been evaluated only in simulation. They also involve complex parameter iteration and model identification, complicating deployment and limiting real-time execution on embedded hardware. In this study, a heavy, 7 m-class underactuated AUV was used to assess a controller for GPS-based positioning and path following through both simulation and lake trials. Threshold filtering, output limiting, and anti-windup are combined without complex calculations involving coupled models. The controller derives the path error from GPS geometry and resets the error to suppress positioning noise. Limits on the output and integral accumulation address overshoot and oscillations. Stable and practically useful control was obtained in both tests, despite the vehicle's substantial inertia and the complex environmental disturbances.

2. Modeling of the Underactuated AUV System

2.1 Coordinate System Definitions

Two standard coordinate systems, shown in Figure 1, were established to describe the planar motion of the underactuated AUV and its position relative to the path in GPS-based positioning and horizontal-plane path-following applications [7]. The global earth-fixed frame O−xy has its origin at a reference point on the water surface, with the x-axis pointing east and the y-axis pointing north. It describes the desired path and the AUV's absolute position. The body-fixed frame B−$x_b y_b$ is attached to the AUV's center of gravity, with the x_b-axis pointing toward the bow and the y_b-axis toward starboard. It is used to describe vehicle attitude and control inputs.

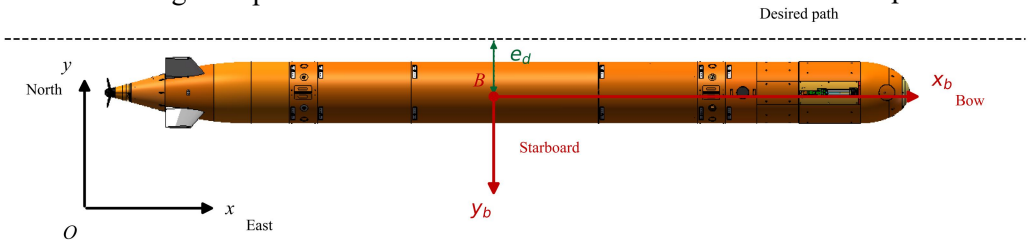


Figure 1. Coordinate Systems for Horizontal-Plane Motion of the Underactuated AUV

2.2 Motion Characteristics of the Underactuated AUV

Surge, sway, and yaw constitute the vehicle's three horizontal-plane degrees of freedom. Only surge thrust and yaw moment are available as control inputs, so sway cannot be controlled independently. A cross-track error cannot therefore be removed by commanding a lateral displacement. The AUV has to turn toward the path and move forward to regain it. This maneuver delays the correction and can carry the vehicle beyond the path, leading to oscillations. Smooth corrective motion must be achieved within these actuation constraints.

Neglecting vertical motion, attitude oscillations, and weak lateral-current disturbances, and considering the vehicle's constant-speed operation, a simplified three-degree-of-freedom kinematic model was established for horizontal-plane motion:

$$\begin{cases} \dot{x} = u\cos\psi - v\sin\varphi \\ \dot{y} = u\sin\psi + v\cos\psi \\ \dot{\psi} = r \end{cases} \quad (1)$$

Here, x and y are the AUV position coordinates in the global frame; u and v are the surge and sway velocities, respectively; ψ is the heading angle; and r is the yaw rate. During low-speed, constant-speed operation, the velocity induced by lateral-current disturbances is very small, so $v \approx 0$ can be assumed, giving the simplified kinematic model:

$$\begin{cases} \dot{x} = u\cos\psi \\ \dot{y} = u\sin\psi \\ \dot{\psi} = r \end{cases} \quad (2)$$

Accounting for hydrodynamic damping and rotational inertia gives the following simplified dynamic model:

$$\begin{aligned} m\dot{u} &= X_u u + X_{|u|u}|u|u + \tau_u \\ I_z\dot{r} &= N_r r + N_{|r|r}|r|r + \tau_r \end{aligned} \tag{3}$$

Here, m is the AUV mass; I_z is the moment of inertia about the vertical axis; X_u and $X_{|u|u}$ are the surge damping coefficients; N_r and $N_{|r|r}$ are the yaw damping coefficients; and τ_u and τ_r are the surge thrust and yaw control moment, respectively. Path corrections are achieved solely through the yaw moment while forward speed remains constant. This avoids complex parameter identification and supports real-time controller operation [8].

3. Path Error Modeling Based on GPS Geometry

Unlike conventional error models based on coordinate differences [9], the proposed approach uses practical GPS positioning logic to formulate a geometric error model for a straight-line path defined by two points. Heron's formula [10] gives the perpendicular distance, while a vector cross product determines the side of the path on which the AUV lies. This provides an accurate, practical, model-free error calculation suited to embedded control [7,8].

3.1 Definition of Path Geometry Parameters

Let the desired straight-line path be defined by two GPS coordinate pairs: the start point $P_1(lat_1, lon_1)$ and the end point $P_2(lat_2, lon_2)$. The AUV's current position is $P_3(lat_3, lon_3)$. To account for the different distance scales of latitude and longitude, the geographic coordinates are first converted to local east-north coordinates:

$$E_i = R(lon_i - lon_0)\cos(lat_0) \tag{4}$$

$$N_i = R(lat_i - lat_0) \tag{5}$$

Here, R is the Earth's radius, and (lat_0, lon_0) is the local reference point, which may be chosen as the path start point P_1. The perpendicular distance from the AUV to the desired path and its position to the left or right of that path are used as path-following error inputs.

3.2 Calculation of Cross-Track Error

Heron's formula is applied to the geometry of the three points to calculate the perpendicular distance from the AUV to the target path. The three side lengths of the triangle are defined as follows:

$$a = |P_1P_3|, b = |P_2P_3|, c = |P_1P_2| \tag{6}$$

With the semiperimeter $p = (a + b + c)/2$, the area of the triangle is:

$$S = \sqrt{p(p-a)(p-b)(p-c)} \tag{7}$$

The unsigned perpendicular distance from the AUV to the desired path is then obtained as:

$$e_d = \frac{2S}{c} \tag{8}$$

3.3 Determining the Side of the Path Using a Vector Cross Product

To select the direction of correction, the planar vector cross product is used to determine whether the AUV lies to the left or right of the path. In local east-north coordinates:

$$s = (E_2 - E_1)(N_3 - N_1) - (N_2 - N_1)(E_3 - E_1) \tag{9}$$

The signed path error is defined from the cross-product result as follows:

$$e = \begin{cases} +e_d, s > 0 \text{(Left of the path; apply a rightward correction)} \\ -e_d, s < 0 \text{(Right of the path; apply a leftward correction)} \\ 0, s = 0 \text{(On the path)} \end{cases} \tag{10}$$

3.4 Error Threshold Filtering

To suppress unnecessary high-frequency corrections caused by small GPS positioning errors, an error threshold E_{th} is introduced, giving the following piecewise error-screening rules:

$$e_c(k) = e(k), |e(k)| \geq E_{th} \tag{11}$$

$$e_c(k) = 0, |e(k)| < E_{th} \tag{12}$$

When the path-following error is below the threshold, the AUV is considered to be within the allowable error band. The current heading is maintained, and the PID integral term and stored derivative states are reset to zero. This suppresses high-frequency chattering and improves the smoothness of steady-state motion [10]. To prevent abrupt changes in the derivative term when switching at the threshold, a first-order low-pass filter is applied to its input:

$$e_f(k) = 0.7e_f(k-1) + 0.3e_c(k) \tag{13}$$

Hysteresis may also be introduced to avoid frequent switching: correction stops when $|e| < E_{th}$, and PID computation resumes when $|e| > 1.25E_{th}$.

4. Design of the Threshold-Limited PID Controller

4.1 Control Challenges

For an underactuated AUV, a corrective command does not produce an immediate change

in path error. This delay makes overshoot and oscillation difficult to avoid with conventional PID. GPS errors create a further difficulty: small fluctuations can trigger repeated adjustments, consuming resources and producing chattering. At large errors, an unconstrained integral term can accumulate excessively; without output limits and anti-windup, the resulting correction may be too large and amplify oscillations about the path. These considerations led us to revise the error filtering and PID computation and to constrain both the output and integral accumulation [1,4].

4.2 Overall Control Architecture

GPS-based geometric error is the sole input to the closed-loop controller; the output is an angle by which to correct the heading. GPS acquisition and geometric error calculation begin each control cycle. The threshold rule selects the effective error for a positional PID calculation with anti-windup, after which the output is limited. Normalizing and updating the heading completes the cycle. As the AUV moves, the sequence is repeated to close the feedback loop. The calculation is simple enough for real-time embedded control and does not depend on an accurate dynamic model.

4.3 Positional PID Control and Anti-Windup

We use a positional PID algorithm for real-time embedded control. Its input is the filtered effective error $e_c(k)$, and its discrete form is:

$$u(k) = K_P e_c(k) + K_i T_s \sum_{j=0}^{k} e_c(j) + \frac{K_d}{T_s}[e_c(k) - e_c(k-1)] \quad (14)$$

Here, T_s is the control period, and K_p, K_i, and K_d are the proportional, integral, and derivative gains, respectively. The proportional term responds rapidly to the instantaneous path error; the integral term eliminates residual steady-state error; and the derivative term anticipates changes in the error, suppressing the inertial lag and dynamic oscillations of the heavy, 7 m-class AUV.

When the error is large, continued accumulation of the integral term can saturate the output and cause path overshoot. The following anti-windup constraint limits this accumulation:

$$I(k) = \text{sat}(I(k-1) + K_i T_s e_c(k), -I_{\max}, I_{\max}) \quad (15)$$

For convenience, the symmetric saturation function is defined as follows:

$$\text{sat}(u, -u_{\max}, u_{\max}) = \begin{cases} u_{\max}, u > u_{\max} \\ u, |u| \le u_{\max} \\ -u_{\max}, u < -u_{\max} \end{cases} \quad (16)$$

Threshold filtering keeps random high-frequency GPS noise from being amplified by the derivative term. Rejecting this noise substantially improves control stability under real-world operating conditions on the water.

4.4 Output Limiting to Prevent Overshoot

Because inertial lag leaves an underactuated AUV prone to overshoot, we place a hard limit on the magnitude of the PID heading correction:

$$u(k) = \text{sat}(u_{raw}(k), -u_{\max}, u_{\max}) \quad (17)$$

Before limiting, the PID output is $u_{raw}(k)$; the maximum permitted heading correction is u_{max}, set here to 30°. For large errors, the limit effectively prevents excessive corrections from carrying the AUV across the desired path and into repeated back-and-forth oscillation. The combination of output limiting and anti-windup suppresses path overshoot caused by integral windup.

4.5 Heading Angle Normalization

The heading angle is periodic over 0°–360°. At the interval boundaries, the output heading is therefore wrapped as follows:

$$\psi_d = \text{mod}(\psi_d, 360^\circ) \quad (18)$$

The normalized heading lies in (0°, 360°], avoiding angular overflow and the erroneous control actions that could result.

4.6 Controller Execution Sequence

In the execution sequence shown in Figure 2, the newly acquired GPS coordinates are first converted to local coordinates. Heron's formula and the vector cross product then supply the signed path error. The threshold rule filters positioning noise, resets inactive PID states to zero, and passes the effective error to the positional PID calculation. Anti-windup is applied within that calculation, and the resulting output is limited before the heading is normalized and updated. Repeating these operations as the vehicle's position and attitude change closes the path-following loop.

5 Comparative Analysis of Simulation and Field Trial Results

5.1 Simulation Platform and Parameter Settings

A numerical simulation platform for a 7 m-class underactuated AUV was developed in MATLAB/Simulink. The model used the actual

vehicle's dimensions and mass: 7 m in length, 533 mm in diameter, and 1260 kg. The vehicle has an underactuated configuration with X-configured rudders and relies solely on yaw moment and longitudinal propulsion for motion control. Discrete-time iterations were run at a control period of 0.25 s for a total of 200 s. During the simulated straight-line path-following task, the longitudinal speed remained constant at 1.7 kn.

The simulations and lake trials used the same controller settings. With angles expressed in degrees, the PID gains were $K_p = 3.0$, $K_i = 0.15$, and $K_d = 0.5$. The path error threshold was $E_{th} = 2$ m, the maximum heading correction was $u_{max} = 30°$, and the integral saturation limit was $I_{max} = 30°$. For comparison, conventional positional PID retained exactly these parameter values but operated without error thresholding, output limiting, or anti-windup. GPS positioning disturbances were represented in the simulation by Gaussian white noise, corresponding to the effective positioning noise left in the integrated navigation output.

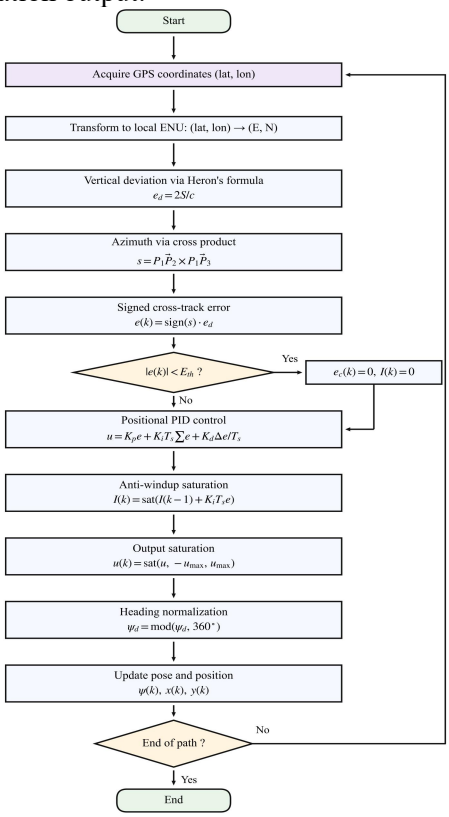


Figure 2. Flowchart of the Threshold-Limited PID Controller Using GPS-Based Geometric Error

5.2 Lake Trial Platform and Parameter Settings

Experimental validation was conducted using an in-house-developed, 7 m-class medium-sized underactuated AUV and data collected during lake trials. The test AUV had an overall length of 7 m, a mass of 1260 kg, and a hull diameter of 533 mm. It used a typical underactuated configuration comprising X-configured rudder surfaces and a single stern-mounted main thruster, with no independent lateral propulsion or lateral rudder-control mechanism. Vehicle attitude was adjusted solely through longitudinal thrust and the equivalent yaw moment generated by the coupled action of the four rudders. Its motion characteristics therefore closely matched the underactuated modeling assumption of heading-only correction with no lateral control input.

Single-point GPS positioning on the test AUV had a raw horizontal accuracy of approximately 2.5 m (1σ). For the path-following error calculation, however, position was taken from the integrated GPS/INS/DVL navigation output. Kalman filtering reduced the effective positioning noise to less than 1 m, making a 2 m error threshold and submeter steady-state accuracy within the threshold band achievable in practice.

The field trials took place in open lake waters, where GPS satellite signals were stable throughout and unobstructed by mountains or shore-based features. The AUV autonomously followed a piecewise-linear mission path specified by latitude and longitude coordinates, with no human intervention during the run. GPS position, path error, heading and attitude, and propeller rotational speed were sampled and recorded together at a high rate.

The lake trials used fixed control settings, with a navigation and control update period of $T_s = 0.25$ s (4 Hz). A constant main-thruster speed of 250 r/min gave a longitudinal speed of approximately 1.72 kn. The error threshold and heading correction limit were set to $E_{th} = 2$ m and $u_{max} = 30°$, respectively, and the PID gains were $K_p = 3.0$, $K_i = 0.15$, and $K_d = 0.5$. The trial lasted approximately 712 s and produced 2845 valid samples as the AUV followed the predefined four-waypoint piecewise-linear trajectory autonomously, without human intervention.

5.3 Metrics for Evaluating Path-Following Performance

Five metrics were used to evaluate the path-following response: (1) maximum tracking error, E_{max}, defined as the largest cross-track deviation from the desired path over the entire mission; (2)

mean steady-state error, E_{avg}, calculated as the mean deviation after the AUV has converged into the path-following band; (3) root mean square error, RMSE, which describes overall tracking smoothness and error dispersion; (4) overshoot, σ, defined by the largest deviation on the opposite side of the desired path after the first crossing; and (5) convergence time, T_c, measured from the maximum initial error to entry into the error threshold band. For convergence to be counted, the error must then remain within that band until the simulation ends.

5.4 Simulation Scenarios and Comparative Results

Starting 20 m from a fixed straight-line path, the simulated AUV was required to converge to and follow that path. The same task was run with conventional positional PID control and with the proposed threshold-limited PID controller. Their simulated performance metrics are compared in Table 1.

Table 1. Simulated Performance Metrics for Conventional PID and the Proposed Threshold-Limited PID Controller

Control algorithm	Max. Error (m)	Overshoot (m)	Convergence time (s)	Steady-state RMSE (m)	Steady-state chattering
Conventional PID	20.00	10.30	110	0.82	Pronounced overshoot and steady-state chattering
Proposed threshold-limited PID	20.00	0.40	62	0.35	No noticeable chattering; stable response

Note: Convergence time is measured at the first entry into the ±2 m threshold band after which the error stays within the band for the rest of the simulation. With conventional PID, the error first entered the band at approximately 50 s, but subsequent integral windup drove the AUV across the path to an error of −10 m. The error did not remain within the band until approximately 110 s; the recorded convergence time was therefore 110 s.

The two controllers responded differently to the large initial error. Under conventional PID, integral windup produced substantial overshoot, followed by repeated path crossings and severe oscillations during convergence. The largest deviation on the opposite side of the path was 10.3 m. Under threshold-limited PID, anti-windup and the 30° heading correction limit prevented excessive integral accumulation. The error decreased monotonically into the ±2 m band and remained there, never overshooting to the other side. Relative to conventional PID, path overshoot was thus nearly eliminated and convergence speed improved by approximately 43%. The steady-state RMSE decreased from 0.82 m to 0.35 m, with complete suppression of steady-state chattering. The simulation therefore supports the theoretical advantages of the algorithm and the validity of the control design.

The contrast is visible in the error histories in Figure 3. With conventional PID, integral windup drove the error to −10.3 m on the opposite side of the path. This pronounced undershoot was followed by a rebound, and small-amplitude chattering persisted at steady state. Threshold-limited PID instead brought the error rapidly and smoothly into the steady-state band, with no overshoot or subsequent loss of stability. This behavior was consistent with the inertia-related control characteristics of a heavy underactuated AUV.

The simulated response reflects the combined action of the controller's modifications. Output limiting and anti-windup suppress overshoot and oscillation while the error is large. Once the AUV reaches steady state, thresholding stops unnecessary corrections and eliminates chattering. During this process, the low-pass-filtered derivative term anticipates changes in error and suppresses the effects of inertial lag. Together, these modifications enable smooth, accurate path following by the underactuated AUV.

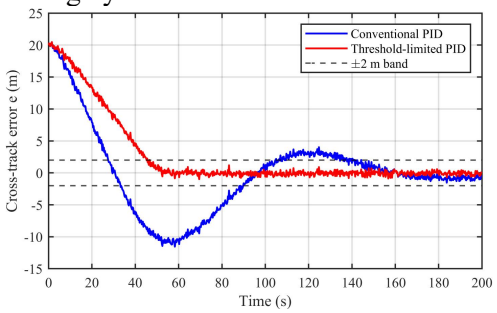


Figure 3. Simulated Path-Following Error Curves under Conventional PID and Threshold-Limited PID Control

5.5 Verifying the Need for Error Thresholding in Simulation

The role of error thresholding was examined in a separate simulation incorporating residual positioning errors representative of integrated

navigation outputs. GPS noise with a standard deviation of 1.0 m was superimposed on a slow random-walk drift bounded by ±1.5 m. Three controllers were tested against this same noise sequence: (1) conventional PID, without a threshold, output limiting, or anti-windup; (2) limit-only PID, with the output bounded by ±30° and no error threshold; and (3) threshold-limited PID, which combined the ±30° output bound with a 2 m error threshold. Table 2 reports their performance over the steady-state interval (t > 100 s).

Table 2. Steady-State Performance Metrics of the Three Controllers (t > 100 s)

Algorithm	RMSE/m	Standard deviation/m	Peak-to-peak value/m	Number of control actions
Conventional PID (no threshold or output limit)	~7.0	~3.0	~15	>200
Limit-only PID (no threshold)	~0.8	~0.7	~3.5	~150
Threshold-limited PID (proposed)	~0.1	~0.1	~0.5	<5

The three controllers' error and heading correction angle responses are plotted in Figure 4. The full time histories, covering 0–200 s, appear in Figures 4(a) and (b); Figures 4(c) and (d) enlarge the steady-state interval from 120–160 s.

The full time histories in Figures 4(a) and (b) show that conventional PID, without a threshold or output limiting, produces reverse overshoot beyond −10 m during initial path acquisition from a large error because of integral windup. After this overshoot, the error continues to oscillate within ±5 m for an extended period. Large heading correction swings within ±60° persist throughout the run. With limit-only PID, which has no threshold, the ±30° output limit suppresses large overshoot, and the error first enters the threshold band within approximately 60 s. However, high-frequency chattering persists in both the error and the heading correction angle during the steady-state interval. With the proposed threshold-limited PID, the error converges monotonically and remains stable after entering the ±2 m threshold band at approximately 60 s; the heading correction angle is nearly zero within the band.

The enlarged steady-state curves in Figures 4(c) and (d) further show that conventional PID has peak steady-state errors of ±6 m, with the heading correction angle continuously oscillating within ±8°. With limit-only PID, the error exhibits high-frequency chattering within ±3.5 m, and the heading correction angle changes continuously within ±7°, leaving the rudder servo in a prolonged state of adjustment. Under the proposed threshold-limited PID controller, by contrast, the error stays within ±0.5 m and its curve is almost horizontal. With the heading correction angle remaining near 0°, the rudder servo is essentially inactive.

Output limiting alone leaves a steady-state error standard deviation of 0.7 m and requires more than 150 control actions. With a 2 m error threshold added, the standard deviation falls to 0.1 m and the number of actions to fewer than 5. Thus, threshold filtering is essential to suppress high-frequency GPS noise and avoid unnecessary rudder movements. Output limiting and thresholding serve distinct purposes: the former prevents overshoot when the error is large, whereas the latter prevents chattering when it is small.

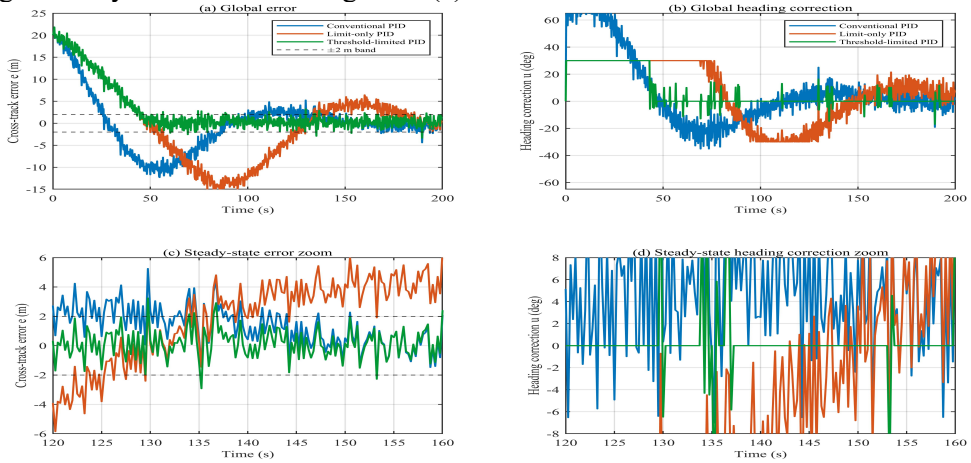


Figure 4. Comparison of Errors and Heading Correction Angles for the Three Controllers: (a) Full Error Time Histories; (b) Full Heading Correction Angle Time Histories; (c) Enlarged Steady-State Error Curves; (d) Enlarged Steady-State Heading Correction Angle Curves

5.6 Lake Trial Setup

Waypoint 1: 116.963940° E, 38.579720° N;
Waypoint 2: 116.963720° E, 38.577290° N;
Waypoint 3: 116.964510° E, 38.577320° N;
Waypoint 4: 116.964780° E, 38.579620° N.

The lake trial required the 7 m-class underactuated AUV to navigate autonomously around the closed piecewise-linear route defined by the four waypoints. No manual intervention was used. Propeller speed was fixed at 250 r/min, while vehicle speed was held at 1.72 kn. Repeated segment transitions and sharp heading changes tested the controller under typical operating conditions, in the presence of weak natural currents and random GPS positioning noise. Throughout the trial, the cross-track error threshold remained E_{th} = 2 m, and each control update allowed a heading correction of no more than 30°.

5.7 Quantitative Analysis of Lake Trial Results

Table 3. Statistics of Measured Cross-Track Errors

Statistic	Full-run data	Steady-state samples within the threshold (|e|≤ 2 m)
Number of samples	2845	2458
Maximum cross-track error/m	10.10	2.00
Minimum cross-track error/m	−10.10	−2.00
Mean cross-track error/m	−0.37	0.01
Mean absolute cross-track error/m	1.33	0.83
Root mean square error (RMSE)/m	2.13	0.96
Standard deviation/m	2.10	0.96
Proportion with absolute error ≤ 2 m	86.40%	100%

Table 4. Statistics of Error-Correction Intervals with Cross-Track Errors Exceeding the Threshold (|e| > 2 m)

Interval number	Time range/s	Duration/s	Maximum cross-track error in interval/m
1	11.0~60.0	49.0	10.10
2	86.0~95.0	9.0	3.30
3	356.0~358.0	2.0	3.30
4	371.0~379.0	8.0	2.40
5	382.0~390.0	8.0	2.30
6	439.0~443.0	4.0	4.70
7	591.0	<1.0	2.10

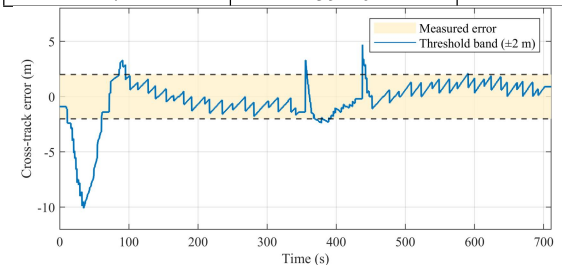


Figure 5. Time History of Measured Cross-Track Error

In Figure 5, the initial approach to the path is followed by generally stable navigation. Over the path-acquisition period (0–60 s), the AUV approached the preset four-waypoint piecewise-linear path from its starting position, with an initial error reaching approximately 10.10 m. Threshold-limited PID achieved convergence in approximately 60 s without significant reverse overshoot. Later error peaks correspond to turns between segments. Once the vehicle entered the next straight segment, the controller quickly brought the error back into the 2 m threshold band without intervention. The measured track in Figure 6 contains four path segments separated by three turns; the error distribution in Figure 7 is concentrated within ±2 m.

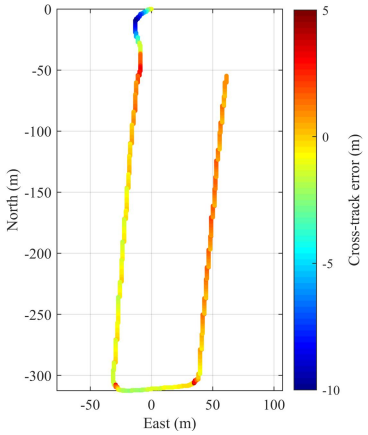


Figure 6 Measured AUV Track (Colors Indicate Cross-Track Error)

Of the 2845 samples collected over the full lake trial, 86.40% had absolute cross-track errors no greater than 2 m (Table 3). For steady-state samples inside the threshold band, the mean absolute error was 0.83 m and the RMSE was 0.96 m, with a standard deviation of 0.96 m. These submeter error statistics indicate consistently high steady-state accuracy under the 2 m threshold constraint, without high-frequency

chattering. The maximum error of 10.10 m and the full-run RMSE of 2.13 m arose mainly from initial path acquisition and the 7 above-threshold intervals, when the vehicle performed maneuvers required in actual operation. A direct comparison of the steady-state RMSE values in Tables 1 and 3 is not appropriate: operating conditions differed between the simulation and the lake trials.

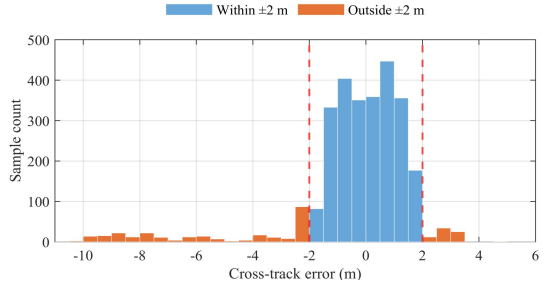


Figure 7. Histogram of Cross-Track Error Distribution

The 7 above-threshold intervals (|e| > 2 m) listed in Table 4 distinguish initial path acquisition from subsequent turning maneuvers. In interval 1, the error reached 10.10 m, and correction took 49 s. Intervals 2–7 occurred as the vehicle turned between segments of the preset piecewise-linear path and reflect normal deviations during operation. For every turn, the maximum error remained within 5 m and correction took less than 10 s, demonstrating rapid recovery after abrupt changes in heading.

5.8 Corroboration between Simulation and Lake Trial Results

Evidence of controller effectiveness is consistent across the numerical simulations and lake trials: the behavior measured on the vehicle closely follows the trends predicted in simulation.

1) Dynamic convergence: During simulated path acquisition from a large initial error, the improved PID controller converges more quickly without significant overshoot. The lake data show a similar response from an initial error of 10.10 m, which decreases smoothly and rapidly without reverse oscillation. This agreement supports the consistent and reliable suppression of inertia-related effects by output limiting and anti-windup in the heavy underactuated AUV.

2) Steady-state smoothness: In simulation, the error converges smoothly without high-frequency steady-state chattering. The lake trial shows the same smooth behavior: the error stays within the 2 m threshold for 86.40% of the operating time, and the steady-state RMSE is as low as 0.96 m. Unnecessary rudder actuation in response to GPS noise is effectively prevented by the threshold-based reset mechanism.

3) Robustness under complex operating conditions: The lake trial extends the ideal straight-line simulation to a piecewise-linear route with multiple turns. These transitions impose abrupt heading changes and transient excessive errors, yet the controller quickly brings the error back within the threshold band. Such rapid recovery provides additional evidence of strong robustness under practical operating conditions.

The lake measurements also validate the three principal features of the control design in practice:

(1) Error threshold filtering keeps GPS positioning noise from triggering unnecessary corrections. Below an error of 2 m, the controller stops producing an output and resets its stored integral and derivative states to zero. Small noise fluctuations therefore cannot build up in the integral term and be amplified. This mechanism is consistent with the measured steady-state response, which shows neither high-frequency chattering nor significant back-and-forth oscillation.

(2) Output limiting and anti-windup suppress inertia-induced overshoot in the underactuated AUV. An initial path-acquisition error of 10.10 m is brought back into the threshold band in approximately 60 s, with no reverse overshoot or back-and-forth oscillation at any stage. Among the 7 above-threshold intervals, every interval after initial path acquisition has a maximum error within 5 m and a correction time below 10 s.

(3) General robustness along a multisegment piecewise-linear path is evident in the measured track, which includes multiple turns at path-segment transitions. After every turn, the controller rapidly restores the error to the threshold band. It thereby accommodates abrupt path changes, weak current disturbances, and GPS sensor noise.

With the error threshold set to 2 m and heading correction limited to 30°, the combined quantitative metrics show rapid convergence from large errors, adaptive error correction during turns, and steady-state navigation without chattering. The proposed improved PID controller delivers this performance at very low embedded computational cost. Its parameters are straightforward to tune, and transfer to practical engineering systems is readily achievable.

6. Conclusions

The threshold-limited PID algorithm developed

in this study addresses overshoot, oscillation, steady-state chattering, and limited disturbance rejection during path following by underactuated AUVs. It obtains both a high-precision path error and the required correction direction from GPS geometry, without a vehicle model. Positioning noise is prevented from causing unnecessary adjustments and high-frequency AUV chattering by error thresholding and a reset mechanism. Output limiting and anti-windup, incorporated into positional PID control, reduce the path overshoot and repeated oscillation associated with inertial lag. The design was validated through comparative simulations and lake trials; the responses observed in both support the proposed control mechanisms.

In simulation, the proposed algorithm reduces path overshoot from 10.3 m to within 0.4 m relative to conventional positional PID. Convergence speed improves by approximately 43%, and the steady-state RMSE falls from 0.82 m to 0.35 m, accompanied by a substantial reduction in steady-state chattering. The lake trials confirm that the algorithm is feasible on an actual underactuated AUV platform. Errors lie within the ±2 m threshold band in 86.40% of all samples, with a steady-state RMSE of 0.96 m within that band. Initial path acquisition produces the maximum error of 10.10 m. Most of the other above-threshold intervals reflect normal operational deviations during turns at path-segment transitions; all of these remaining intervals last less than 10 s.

The algorithm was designed specifically for the inertia and lag characteristics of a 7 m-class, high-mass underactuated AUV. Modeling GPS-based geometric error removes the need for precise dynamic parameters, while threshold filtering, output limiting, and anti-windup jointly mitigate the steady-state chattering, turning overshoot, and unnecessary adjustments associated with conventional PID. Neither complex iterative calculations nor model identification is required. The resulting control structure is simple, has low computational demand, and uses readily tunable parameters. The algorithm has potential for real-time embedded implementation and can effectively improve both the dynamic response and steady-state accuracy of underactuated AUV path following. Future work could introduce time-varying ocean-current disturbances and use intelligent parameter tuning, such as fuzzy adaptation or reinforcement learning, to optimize control performance. Such extensions could further improve the ability of large underactuated AUVs to follow paths accurately and stably in complex marine environments.

References

[1] Er M J, Gong H, Liu Y, et al. Intelligent trajectory tracking and formation control of underactuated autonomous underwater vehicles: A critical review. IEEE Transactions on Systems, Man, and Cybernetics: Systems, 2024, 54(1): 543-555.

[2] MENG F G, LIU A M, HU Y, et al. Overview of autonomous underwater vehicles and their motion control technologies. Journal of Vibration and Shock, 2025, 44(11): 321-338.

[3] WANG F, WAN L, LI Y, et al. A survey on development of motion control for underactuated AUV. Shipbuilding of China, 2010, 51(2): 227-241.

[4] HE L, ZHANG Y, XIE M, et al. Three-dimensional trajectory tracking control of underactuated AUV based on fractional-order PID and super-twisting extended state observer. Fractal and Fractional, 2025, 9(9): 580.

[5] WAN L, ZHANG Y H, SUN Y S, et al. ADRC path-following control of underactuated AUVs. Journal of Shanghai Jiao Tong University, 2014, 48(12): 1727-1731+1738.

[6] YAN Z P, ZHOU J J. Control technology of unmanned underwater vehicles. Beijing: National Defense Industry Press, 2015.

[7] GHOSH P, MANDAL P. AUV way-point tracking at constant velocity: Cross-track error (CTE) and line-of-sight (LOS) guidance. Engineering Research Express, 2024, 6(2): 025207.

[8] FOSSEN T I. Handbook of marine craft hydrodynamics and motion control. Chichester: Wiley, 2011.

[9] LEKKAS A M, FOSSEN T I. Integral LOS path following for curved paths based on a monotone cubic Hermite spline parametrization. IEEE Transactions on Control Systems Technology, 2014, 22(6): 2287-2301.

[10] LIU C, SUN T, WANG X. Constrained LOS guidance for path following of underactuated marine vehicle with input saturation. Ocean Engineering, 2024, 307: 118217.